RESEARCH ARTICLE

Adaptive-Width Generalized Correntropy Diffusion Algorithm for Robust Control Strategy of Microgrid Autonomous Operation

AHMED M. HUSSIEN[1], **HANY M. HASANIEN**[1,2], **(Senior Member, IEEE),**
MOHAMMED H. QAIS[3], **(Member, IEEE),**
AND SAAD ALGHUWAINEM[4], **(Senior Member, IEEE)**

[1]Electrical Engineering Department, Faculty of Engineering and Technology, Future University in Egypt, Cairo 11835, Egypt
[2]Electrical Power and Machines Department, Faculty of Engineering, Ain Shams University, Cairo 11517, Egypt
[3]Centre for Advances in Reliability and Safety, Hong Kong, China
[4]Electrical Engineering Department, College of Engineering, King Saud University, Riyadh 11421, Saudi Arabia

Corresponding author: Hany M. Hasanien (hanyhasanien@ieee.org)

ABSTRACT This study introduces a new method for achieving the robust performance of an isolated microgrid (MG) using an adaptive-width generalized correntropy diffusion algorithm (AWGC-DA). In the approach, the width of the kernel is adjustable, allowing the program to reject misleading input from attackers; the technique may identify attackers using a simple identification rule. The Response Surface Methodology is utilized in combination with three optimization algorithms: the Coot bird metaheuristic optimizer (COOT), the sunflower optimization (SFO), and the particle swarm optimization (PSO) to improve the technique's effectiveness. To assess the effectiveness of the new technique, a standard microgrid is tested under three different scenarios: (1) disconnected from the utility grid (autonomous status); (2) variations in load while in autonomous status; and (3) a three-phase fault while in autonomous status. In addition, numerous simulations are performed using the PSCAD/EMTDC software to verify the efficacy of the proposed technique. The main contribution of this study is to enhance the system transients by minimizing the overshoots, steady state error, and settling time which increases the efficacy of the autonomous MG process. Finally, to demonstrate its validity, the performance of the suggested approach is compared to that of other methods, including the LMSRE-based adaptive control, EBS-ABA, COOT, SFO, and PSO algorithms. The results confirm that the AWGC-DA method outperforms the other methods regarding the system's transient response.

INDEX TERMS Adaptive-width generalized correntropy diffusion algorithm, microgrid, adaptive control.

I. INTRODUCTION

A. PROBLEM STATEMEN

The transformation of decentralized renewable power networks is currently undergoing substantial changes to cope with the surge in the load profile. These developments have yielded technical, scientific, environmental, and economic benefits. However, the load demand is increasing rapidly, underscoring the urgency of replacing centralized power plants with distributed generators (DGs) strategically positioned across distribution networks [1]. Implementing this approach can prove highly effective in minimizing transmission losses and obviating the need for extensive transmission networks. However, to ensure a continuous power supply by the DG units, certain factors must be considered. Consequently, the microgrid (MG) concept has emerged, comprising DGs and their local loads.

MGs are essentially small-scale grid schemes that can be controlled and utilized in one of two ways: grid-tied or grid-off (islanded) mode, as per the electricity requirements [2].

The associate editor coordinating the review of this manuscript and approving it for publication was Ruisheng Diao.

The utility identifies the MG voltage and frequency in the grid-tied status. However, their powers need to be regulated. Conversely, when in islanded mode, the voltage and frequency of the MG need to be adjusted [3]. Thus, it becomes imperative to keep track of the operation of DG units to ensure a continuous power supply to the load.

In off-grid mode, various sophisticated control systems are employed to guarantee adequate and secure operation. These control techniques can be categorized as droop control (DCL), centralized control (CC), and multi-variable and servo-mechanism (MASM) tactics. DCL enables peer-to-peer administration and plug-and-play capabilities by separately controlling the outputs of several DGs, eliminating the need for communication between them. An Active and reactive power DCL-based remote controller technique has been recommended [4]. Moreover, a completely decentralized solution based on dual-frequency-droop regulation has been developed [5]. A notable benefit of DCL is its ability to coordinate distributed units independently, thereby improving resilience and dependability compared to earlier power-sharing and MG frequency-regulating techniques. Nevertheless, with smaller-voltage MGs, line impedance has a major impact on control efficiency, which causes power coupling [6]. To address this issue, the imaginary vectors conversion method has been enhanced [7], even though it may have an impact on dependability. In contrast, CC techniques need higher bandwidth links, and any disturbance in these networks could end up with an MG failure. Therefore, a CC scheme for DC MG constructed on autonomous communications has been developed and implemented [8]. Lastly, an innovative approach for developing MASM systems with many inputs and outputs, as well as open-loop system control, has been provided [9]. Nonetheless, its vast complexity is a hurdle.

Of its significant stabilization borders, the proportional-integral controller (PI-C) is frequently employed for nonlinear systems. However, it falls into deficiencies regarding variant parameter tolerance and system nonlinearities. As a result, determining the optimum PI configuration in this system is a substantial task. Significant efforts have been undertaken in recent years to build the perfect MG controller to provide a stable system. When the system is believed to be linear, PI-Cs employ a dq converter to modify the converter's output voltage [10], and they are adjusted using simple processes like the Ziegler-Nichols approach [11]. The PI-C, on the other hand, delivers saturated outcomes, lowering system durability through a more significant phase lag. Controllers react promptly to changes in parameters and operating situations [12]. An autonomous PI-C for controlling a hybrid power network has been presented in [13]. In addition, numerous metaheuristic algorithms that replicate natural or physical phenomena are capable of solving objective functions.

Natural phenomena like animals, humans, and science Natural phenomena like animals, humans, and science are used to develop metaheuristic techniques [14].

Enhanced Transient Search Optimization for power flow problems [15]. Developed Circle Search Algorithm for optimal power flow problem [16]. A hybrid optimization based on machine learning and transient search optimization to resolve the optimum power flow issue [17]. To determine the design factors of proton exchange membrane fuel cells, the Enhanced Bald Eagle Search Algorithm is used. [18]. Furthermore, numerous optimization approaches, such as genetic algorithms [19], [20], [21], chaotic map-based chameleon Swarm Algorithm [22], the Sunflower (SFO) algorithm [23], Artificial Rabbits Optimizer [24], the Cuttlefish optimization algorithm [25], the particle swarm optimization (PSO) [26], [27], [28], [29], particle swarm optimization-gravitational search algorithm [30], Artificial Fish Swarm Algorithm [31], and improved Mutation particle swarm optimization [32]. Many of these approaches possess both advantages and challenges [33]. However, we are still a long way from establishing a comprehensive universal benchmark for the MG system.

B. LITERATURE SURVE
Even though optimization approaches are effective and resilient implements for creating PI-Cs, they have substantial limitations, including a problematic methodology, a high memory requirement, and a more extended optimization procedure. Therefore, the adaptive PI-C is an excellent alternative for modifying PI-C settings in real time without using any optimization approaches. This cuts down on the duration dedicated to the structure and the effort put into this challenge. Furthermore, multiple adaption strategies were applied to fine-tune the PI-C. Adaptive control (ACL) is proposed based on an affine projection method and has a faster convergence time and less system complexity than optimization approaches [34]. It also has several visually pleasing aspects, such as the coefficient vector. Furthermore, this technique consistently obtains correct data regardless of the variables, as explained in [35] and [36] presents a unique ACL outperforming previous techniques by leveraging a set-membership engine approach. A pole-shifting self-tuning ACL was also used to improve the dynamic response of two linked autonomous MGs [37]. An adaptive PI controller has been implemented with The least mean and the square root of exponential (LMSRE) algorithm to calculate controller parameters for improving autonomous microgrid operation efficiency in [38]. The introduction of an actual negative error normalizes this technique. LMSRE also provides fast convergence and dependability with little error. The continuous P norm hybrid technique is introduced as a unique ACL that rapidly updates the fuzzy controller structure [39]. In [40], A cascaded control approach with an improved multiband structured sub-band adaptive filter technique is applied to alter voltage source converters. A fuzzy PI controller-based model, reference ACL, is proposed for improving the dynamic performance of many linked MGs using the coronavirus herd immunity

optimizer [41]. Reference [42] describes a new approach for optimal management of an islanded MG based on an improved block-sparse adaptive Bayesian algorithm (EBSABA). The benefits of the EBS-ABA include fast convergence, a simple approach, and reduced computational complications. Conventional adaptive methods have been outperformed by the Adaptive-Width Generalized Correntropy Diffusion Algorithm (AWGC-DA) [43], and we propose using the GC kernel cost function to render the DA concurrently reliable against impulsive noise and incorrect information insertion attack. In the technique, the width of the kernel is adjustable, allowing the program to reject misleading input from attackers. The technique may identify attackers using a simple identification rule that compares the width of the kernel to a limit. This is the crucial reason why the authors employed this outstanding durability approach for continuous modification of the DGs' PI-C gains.

C. THE MAJOR CONTRIBUTION

This study contributes to that pool by presenting a novel method for optimal control of off-grid MGs based on the AWGC-DA. To increase the efficacy of the autonomous MG process, this work applies this adaptive approach in a PI-C optimal control strategy with numerous PI-C parameters. Multiple simulations illustrate the usefulness of the suggested AWGC-DA in the scheme's transient responses over LMSRE-based ACL, EBS-ABA, and other non-adaptive methods, like the COOT, SFO, and PSO techniques, to validate the suggested approach.

The presented work assists in filling the gaps that have already been demonstrated by:

1) investigating the recently proposed AWGC-DA method on an altered PI-C to improve MG efficacy,
2) Demonstrating the viability of the novel method by examining the MG during three distinct operating scenarios:
   a) Isolated from the utility (off-grid mode);
   b) Load changes during off-grid mode; and
   c) a symmetrical fault under the off-grid mode.
3) Prove the superiority of the offered adaptive technique using a comparison study with other optimization methods.

This is how the following sections of the paper are arranged. The MG modeling is shown in the second section. The control mechanism is described in the third section. The method structures are depicted in the fourth section. The fifth section depicts conventional optimization strategies and procedures involved in modeling. In the sixth section, we present and discuss the results obtained from the simulations. Finally, the conclusion is given in the final paragraph.

II. MG MODELING

Figure 1 displays an MG that has been essentially divided into three DGs coupled through transmission wires. Through PCC 1, transmission wires connect the main grid to the DGs.

TABLE 1. MG data.

Transformer	$\Delta/Y = 600V/13.8$ KV
Load	C_1, C_2, and $C_3 = 50$, 42, and 33 μF
	R_{l2}, R_{l1}, R_{22}, and $R_{33} = 150$, 9, 5, and 20 Ω
	L_l, L_2, and $L_3 = 0.6$, 0.4, 1.5 H
Transmission Line (Z_{TL1}, and Z_{TL2})	R_{TL1}, and $R_{TL2} = 0.7$, and 1.5 Ω
	L_{TL1}, and $L_{TL2} = 0.5$, and 0.9 mH
Filter (Z_f)	$R_f = 1.5$ mΩ, $X_f = 0.5$ mH
Grid	V = 13.8 KV, $R_g = 0.2$ Ω, $L_g = 0.3$ mH

To avoid unneeded power quality issues, each DG has a DC supply linked to pulse width modulation (PWM) and linked to a transformer by a filter. Following the Δ-Y transformer, RLC load is applied. Table 1 contains the MG information.

The suggested MGs can be controlled and utilized in either: grid-tied or grid-off status, per the electricity requirements. The utility identifies the PCC voltage and frequency in the grid-tied status. However, their powers need to be regulated. Conversely, when in islanded mode, the voltage and frequency of the MG need to be adjusted. Thus, it becomes imperative to keep track of the operation of DG units to ensure a continuous power supply to the load. This paper focuses on increasing MG efficacy in islanded mode by utilizing the cascade control method, detailed in the following section.

III. CONTROL MECHANISM

Each DG has two layers of control relies on the cascading control technique. The outer layer manages active and reactive powers in the grid-tied mode. The inner layer simultaneously tunes the direct and quadrature (d-q) current components ($I_{con.\_d}$, I_{con_q}) to manage the voltages of the PCC. In the autonomous mode, the outer layer regulates both d-q voltages (V_q, V_d), while the inner control layer tunes the d-q currents. The process of transformation for the d-q references voltages ($V_{con.\_d}*$, $V_{con.\_q}*$) provides the reference voltages ($V_{con.\_a}*$, $V_{con.\_b}*$, $V_{con.\_c}*$). The four PIs shown in Figure 2 are used to generate $V_{con.\_d}*$ and $V_{con.\_q}*$. Eventually, the inverter applies a comparator to compare a triangle signal to the reference voltages.

The parameters of the PI-Cs are estimated using AWGC-DA and other techniques. The fourth section goes into further detail about these PI-Cs.

IV. PROCESS OF DESIGN

A. GAINS CONFIGURATION

This research employs six PI-Cs, with each DG using two controllers. Specifically, DG$_1$ employs PI$_{11}$ and PI$_{12}$, DG$_2$ employs PI$_{21}$ and PI$_{22}$, and DG$_3$ employs PI$_{31}$ and PI$_{32}$.

The PI-Cs parameters utilized in this research are the proportional gain (KP) and integral time constants (TI). In particular, PI$_{11}$'s KP is represented by N$_1$, PI$_{11}$'s TI is represented by N$_2$, PI$_{12}$'s KP is represented by N$_3$, and so on, with PI$_{32}$'s KP represented by N$_{11}$ and PI$_{32}$'s TI represented by N$_{12}$.

This study employed three boundaries for the parameters of the controllers, which are presented in Table 2
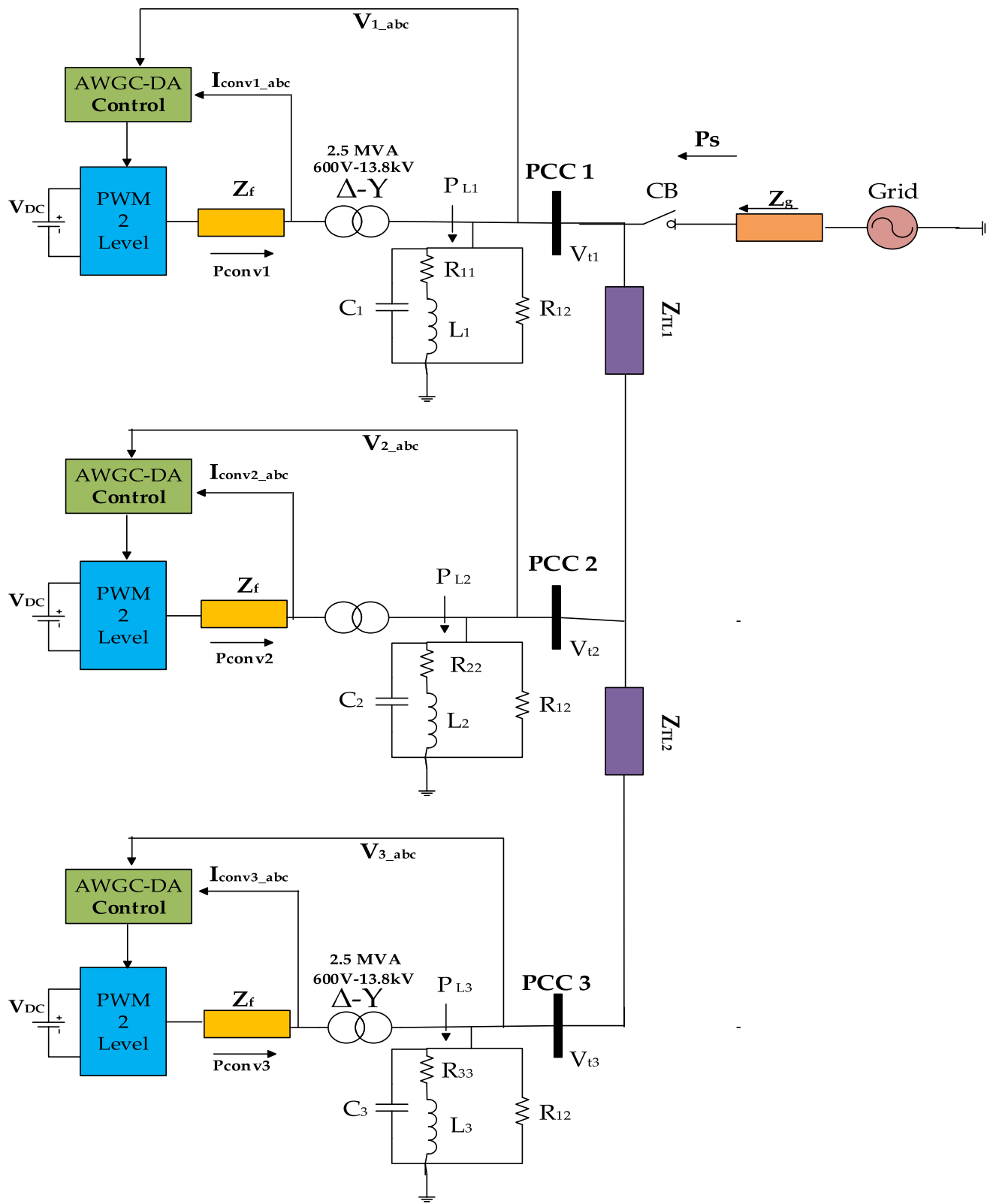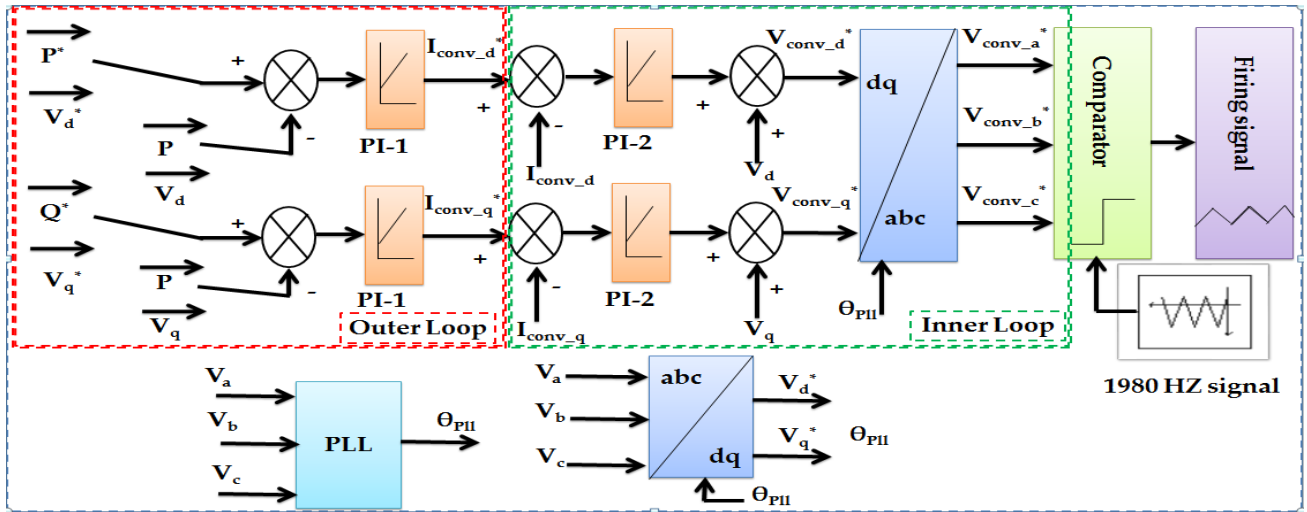
FIGURE 1. MG diagram.

FIGURE 2. The control scheme for islanding MG.

TABLE 2. RSM boundaries.

Gains Levels	(−1)	(0)	(1)
N_1	2.15	4.9	7.65
N_2	0.0008	0.0099	0.019
N_3	1.72	2.387	3.054
N_4	0.057	1.5885	3.12
N_5	1.63	4.435	7.24
N_6	0.00097	0.008385	0.0158
N_7	1.48	2.025	2.57
N_8	0.13	1.4915	2.853
N_9	1.14	3.847	6.554
N_{10}	0.00098	0.00649	0.012
N_{11}	1.252	1.711	2.17
N_{12}	0.0554	1.3427	2.63

The values denoted by levels (-1), (0), and (1) in this context refer to the minimum, mid, and maximum safe values, respectively

B. PSCAD/EMTDC SOFTWARE
PSCAD program is used to model the MG network. The data obtained from those models under various conditions is sent into the response surface methodology (RSM).

C. RSM & MINITAB SOFTWARE
The RSM, a computational technique, employs a robust analytical approach to establish relationships between inputs and outputs [44]. The inputs for the RSM consist of the steady-state error (E_{sse}), maximum overshoot and undershoot percentages (MPOT and MPUT), and settling time (T_{stl}) of the voltage profile. These values are obtained from PSCAD and documented in [11]. To generate the RSM, MINITAB software is utilized.

The objective function for this MG is defined by minimizing G1 (MPOT), G2 (MPUT), G3 (T_{stl}), and G4 (E_{sse}) under the specified conditions. The RSM model used is a second-order polynomial shown in Equation (1).

$$G_y = M_1 + M_2N_1 + M_3N_2 + M_4N_3$$
$$+ M_5N_4 + M_6N_1^2 + M_7N_2^2 + M_8N_3^2$$

$$+ M_9N_4^2 + M_{10}N_1N_2 + M_{11}N_1N_3 + M_{12}N_1N_4$$
$$+ M_{13}N_2N_3 + M_{14}N_2N_4 + M_{15}N_3N_4 \quad (1)$$

where $y = 1, 2, 3, 4$, and $M_1, M_2, M_3 \ldots, M_{15}$ are the predicted RSM coefficients for the conditions described in [11].

V. OPTIMIZATION STAGE
The weight method [45] is utilized in Equation (1) to adjust PI parameters while minimizing transients by considering COOT, SFO, and PSO procedures. Table 3 displays the weights used in this study.

TABLE 3. Weights levels.

Weights (W_{gt})	DG #		
W_{gt1}		MPUT	0.2
W_{gt2}		MPOT	0.2
W_{gt3}	DG_1	T_{stl}	0.075
W_{gt4}		E_{sse}	0.03
W_{gt5}		MPUT	0.125
W_{gt6}		MPOT	0.125
W_{gt7}	DG_2	T_{stl}	0.04
W_{gt8}		E_{sse}	0.02
W_{gt9}		MPUT	0.075
W_{gt10}		MPOT	0.075
W_{gt11}	DG_3	T_{stl}	0.025
W_{gt12}		E_{sse}	0.01

A. THE AWGC-DA ALGORITHM
The primary concept of this algorithm is to apply the generalized Correntropy kernel function to the local cost function of every node. This involves using distinct exponent and width parameters for every node. As a result, the local cost function can be expressed as follows [43]:

$$J_k(\omega) = \sum_{z \in N_k} a_{zk} A_z exp\left(-\left|\frac{e_{z,i}}{\beta_z}\right|^{\alpha_z}\right) \quad (2)$$

where $\beta_z \geq 0$ and $a_z \geq 0$ are the node z's width and exponent parameters, respectively, ω is the unknown vector, e_z is the

error, and $A_z = (\frac{1}{\beta_z})^{\alpha z}$. The same rate exponent coefficient $\alpha z = \alpha$ is considered for each node but a varied width β_z for each of them for ease. As a result, the GC-DA version of the Adapt Then Combine (ATC) is as described below [46]:

$$\begin{cases} \psi_{k,i+1} = \omega_{k,i} + \mu_k \sum_{z \in N_k} a_{zk} f(e_{z,i}) sign(e_{z,i}) U_{z,i} \\ \omega_{k,i+1} = \sum_{l \in N_k} C_{zk} \psi_{z,i+1} \end{cases} \quad (3)$$

where $f(e_{z,i}) = \frac{A_z}{\beta_z} exp\left(-\left|\frac{e_{z,i}}{\beta_z}\right|^\alpha\right) \left|\frac{e_{z,i}}{\beta_z}\right|^{\alpha-1}$

where U is the input signal C_{zk} is the combination coefficients from node z to node k. To improve the GC-DA algorithm's robustness against adversaries, a reduced width parameter β_z is provided to adversaries so that their errors $e_{z,i}$ don't negatively impact the algorithm while in the adaptation phases. As a result, an adaptive-width GCDA algorithm (AWGC-DA) is applied. The disturbance term $\|\psi_{k,i+1} - \omega_{k,i}\|_2^2$ is minimized to get the ideal value for β_z. The width parameter β_D for node D can be obtained by formulating the error $(\psi_{k,i+1} - \omega_{k,i})$ as follows

$$\psi_{k,i+1} - \omega_{k,i} = C_D + \mu_k a_{Dk} f(e_{D,i}) sign(e_{D,i}) U_{D,i} \quad (4)$$

where $C_D = \mu_k \sum_{z \neq D} a_{lk} f(e_{z,i}) sign(e_{z,i}) U_{z,i}$

As a result, the disturbance may be expressed as

$$\|\psi_{k,i+1} - \omega_{k,i}\|_2^2 = \|C_D\|_2^2 + 2\mu U_{D,i} a_{Dk} f(e_{D,i}) \\ sign(e_{D,i}) U_{D,i} + \mu^2 a_{Dk}^2 f^2(e_{D,i}) U_{D,i} \quad (5)$$

Considering that β_D is the only variable that needs to be found and that the rest of the parameters are constant and termed, minimizing the disturbance term in (5) equals to minimizing the next equation.

$$G_D(D) = b_{D,i} f_D(e_{D,i}) sign(e_{D,i}) + d_{D,i} f^2(e_{D,i}) \quad (6)$$

where $b_{D,i} = 2a_{Dk} U_{D,i}, d_{D,i} = \mu a_{Dk}^2 U_{D,i}$, and

$$f_D(x) = \frac{A_D}{\beta_D} exp\left(-\left|\frac{x}{\beta_D}\right|^\alpha\right) \left|\frac{x}{\beta_D}\right|^{\alpha-1}$$

Because the function G_D isn't-convex, we utilize descent gradients to progressively adjust β_D to prevent trapped in local minimums. As a result, we utilize the recursion method below to update β_D.

$$\beta_{D+1} = \beta_D - \mu_\beta \frac{\partial G_D(\beta_D)}{\partial \beta_D} \quad (7)$$

After certain modifications and deleting indices of the functions for ease, and supposing $\frac{\partial e_{D,i}}{\partial \beta_D}$ is a constant term, the recursion in (8) will be identical to that in (8).

$$\beta_{D+1} = \beta_D - \mu_\beta(b_{D,i} f'(e_{D,i}) + d_{D,i} f(e_{D,i})) \quad (8)$$

Some computations result in the following formula for this function's derivatives, resulting in

$$f'(x) = -sign(x) \frac{\alpha A_D}{\beta_D^\alpha} |x|^{\alpha-1} exp\left(-\left|\frac{x}{\beta_D}\right|^\alpha\right) \left|\frac{x}{\beta_D}\right|^{\alpha-1}$$

TABLE 4. The outcomes of each DG for scenario 1 with AWGC-DA, EBS-ABA, LMSRE, COOT, PSO, and SFO techniques.

	AWGC-DA	EBS-ABA	LMSRE	COOT		SFO		PSO	
				Scenario 1 DG 1					
Optimal size	online	online	online	N_1	6.21	N_1	6.421	N_1	2.1472
				N_2	0.0321	N_2	0.0054	N_2	0.00572
				N_3	2.65	N_3	2.952	N_3	1.6791
				N_4	1.91	N_4	0.3472	N_4	0.3392
MPUT	7.391%	8.21%	7.93%	7.423 %		12.93%		20.4%	
T_{stl}	0.031 s	0.037 s	0.045 s	0.0382 s		0.0343 s		0.0562 s	
E_{sse}	0.193%	0.2%	0.34%	0.29 %		0.37%		0.42%	
				Scenario 1 DG 2					
Optimum size	online	online	online	N_5	6.15	N_5	5.982	N_5	1.5692
				N_6	0.0318	N_6	0.0042	N_6	0.00431
				N_7	2.59	N_7	2.5082	N_7	1.2342
				N_8	1.95	N_8	0.299	N_8	0.30572
MPUT	7.37%	8.1%	7.82%	7.434 %		12.54%		20.21%	
T_{stl}	0.0307 s	0.035 s	0.0424 s	0.03827 s		0.0325 s		0.0554 s	
E_{sse}	0.191%	0.19 %	0.32%	0.312 %		0.36%		0.415%	
				Scenario 1 DG 3					
Optimum size	online	online	online	N_9	6.04	N_9	5.5343	N_9	1.07
				N_{10}	0.0307	N_{10}	0.00314	N_{10}	0.0034
				N_{11}	2.51	N_{11}	2.0991	N_{11}	0.995
				N_{12}	1.99	N_{12}	0.2479	N_{12}	0.259
MPUT	7.32%	7.95%	7.64%	7.451 %		12.32%		20.05%	
T_{stl}	0.0304 s	0.034 s	0.0418 s	0.03831 s		0.0319 s		0.0551 s	
E_{sse}	0.189%	0.187%	0.312%	0.289 %		0.354%		0.408%	

$$+ sign(x) \frac{(\alpha-1)A_D}{\beta_D^\alpha} |x|^{\alpha-1} exp\left(-\left|\frac{x}{\beta_D}\right|^\alpha\right) \left|\frac{x}{\beta_D}\right|^{\alpha-2} \quad (9)$$

As well, we have

$$\frac{\partial G_D(\beta_D)}{\partial \beta_D} \propto b_{D,i} f'(e_{D,i}) + d_{D,i} f(e_{D,i}) \quad (10)$$

Then, by substituting (9) for (10) and making some other modifications, we obtain

$$\frac{\partial G_D(\beta_D)}{\partial \beta_D} \propto \frac{A_D}{\beta_D^\alpha} exp\left(-\left|\frac{e_{D,i}}{\beta_D}\right|^\alpha\right) |e_{D,i}|^{\alpha-2} \\ \left[b_{D,i} \left[-\alpha \left|\frac{e_{D,i}}{\beta_D}\right|^\alpha + \alpha - 1\right] 2d_{D,i} |e_{D,i}|\right] \quad (11)$$

As a result, the optimal recursion for β_m is

$$\beta_{D+1} = \beta_D - \mu_\beta \frac{A_D}{\beta_D^\alpha} exp\left(-\left|\frac{e_{D,i}}{\beta_D}\right|^\alpha\right) |e_{D,i}|^{\alpha-2} g_{D,i} \quad (12)$$

where $g_{D,i} = b_{D,i} \left[-\alpha \left|\frac{e_{D,i}}{\beta_D}\right|^\alpha + \alpha - 1\right] 2d_{D,i} |e_{D,i}|$

In this study, all PI parameters are constantly updated in real-time using Equation (12). Moreover, the constants α and μ are set at 5.5 and 0.01, respectively. in this context, the PI-Cs' $k_p(L)$ and $T_i(L)$ are constantly modified by applying the next formulae:

$$k_p(L+1) = k_p(L) - \Delta k_p(L) \quad (13)$$

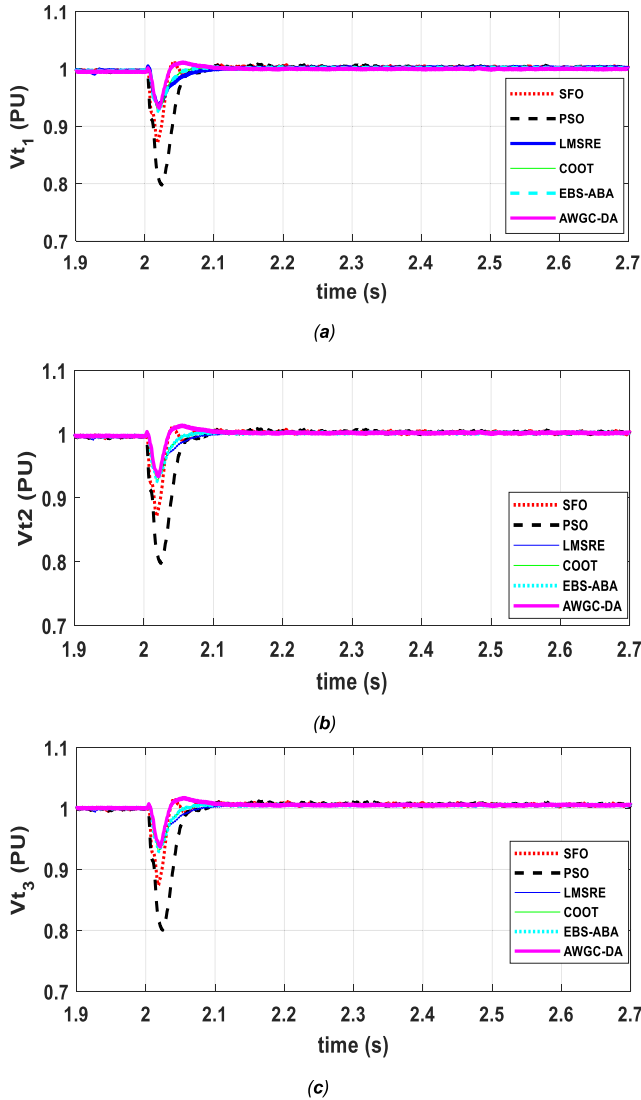$$T_i(L+1) = T_i(L) - \Delta T_i(L) \quad (14)$$

FIGURE 3. The profile voltages of, (a) DG1, (b) DG2, and (c) DG3 for scenario 1 with using AWGC-DA, EBS-ABA, LMSRE, COOT, PSO, and SFO techniques.
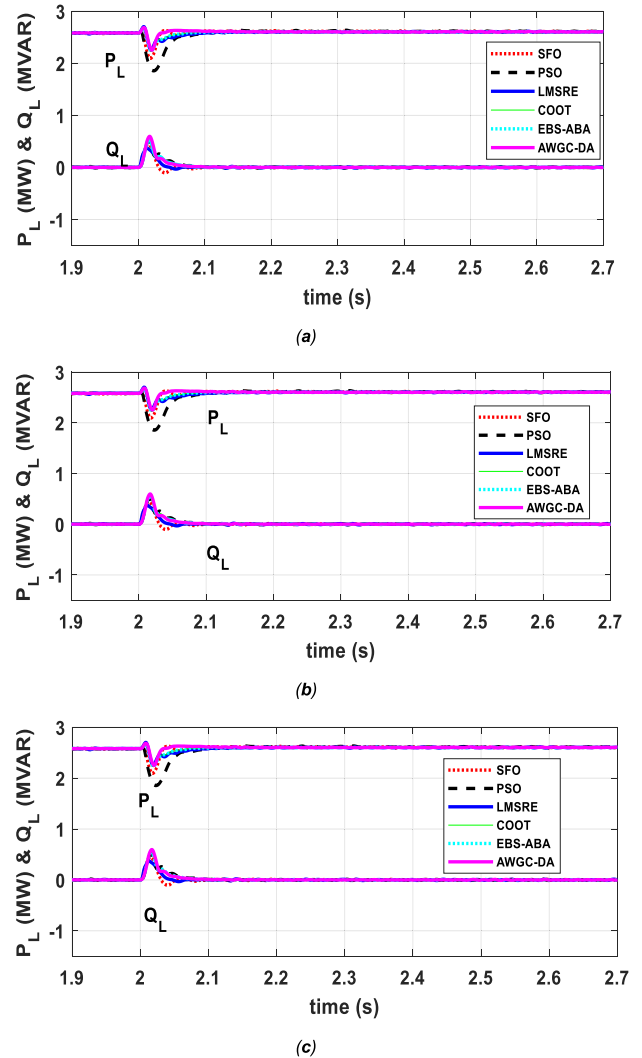

FIGURE 4. The load powers (P&Q) of, (a) DG1, (b) DG2, and (c) DG3 for scenario 1 with using AWGC-DA, EBS-ABA, LMSRE, COOT, PSO, and SFO techniques.

Equations (13)- (14) are utilized to calculate the adjusted parameters of the PI-C

$$\Delta k_p\left(L\right) = \mu_\beta \frac{A_D}{k_p\left(n\right)^\alpha} exp\left(-\left|\frac{e_{D,i}}{k_p\left(n\right)}\right|^\alpha\right)\left|e_{D,i}\right|^{\alpha-2} g_{D,i} \tag{15}$$

$$\Delta T_i\left(L\right) = \mu_\beta \frac{A_D}{T_i\left(n\right)^\alpha} exp\left(-\left|\frac{e_{D,i}}{T_i\left(n\right)}\right|^\alpha\right)\left|e_{D,i}\right|^{\alpha-2} g_{D,i} \tag{16}$$

VI. THE SIMULATIONS' DESCRIPTION AND RESULTS
This part is devoted to determining the results that will validate the cogency and utility of the presented control strategy utilizing the AWGC-DA. The suggested approach's performance is largely judged by its capability to keep the PCC voltages within the allowed ranges during several MG operation scenarios. Furthermore, the simulation outcomes demonstrate the sanity of the controller system, which was

achieved using the PSCAD program. The novel AWGC-DA technique is compared to the results of the previous optimizations reported in [11] and [47] to show its efficiency. Furthermore, a conventional MG is tested under three different scenarios: (1) disconnected from the utility grid (autonomous status); (2) variations in load while in autonomous status; and (3) a three-phase fault while in autonomous status.

A. SCENARIO 1 (AUTONOMOUS STATUS)
In the initial scenario, the MG runs while on the grid-connected status. At 2 seconds, the MG is intentionally disconnected from the grid (autonomous status). The optimum PI gains for the DGs using AWGC-DA, EBS-ABA, LMSRE, COOT, PSO, and SFO techniques are presented in Table 4. The voltage of the DGs using AWGC-DA and the other methods is compared in Figs. 3a-c. Additionally, Figs. 4a-c show the complex power in the DGs using AWGC-DA,

TABLE 5. The outcomes of each DG for scenario 2 with AWGC-DA, EBS-ABA, LMSRE, COOT, PSO, and SFO techniques.

	AWGC-DA	EBS-ABA	LMSRE	COOT		SFO		PSO	
				Scenario 2 DG 1					
Optimal size	online	online	online	N_1	6.374	N_1	6.468	N_1	1.924
				N_2	0.001	N_2	0.0124	N_2	0.0118
				N_3	2.54	N_3	2.2795	N_3	2.3123
				N_4	0.923	N_4	0.2382	N_4	0.2315
MPUT	0.521%	2.314%	1.91%	0.491 %		2.205%		3.271%	
MPOT	0.892%	2.945%	2.216%	0.986 %		2.9671%		3.532%	
T_{stl}	zero	zero	0.4015 s	zero		0.4331 s		0.4531 s	
E_{sse}	0.16%	0.21%	0.425%	0.381 %		0.4531%		0.496%	
				Scenario 2 DG 2					
Optimal size	online	online	online	N_5	6.293	N_5	6.0245	N_5	1.4025
				N_6	0.0012	N_6	0.0097	N_6	0.0103
				N_7	2.511	N_7	1.8615	N_7	1.7983
				N_8	0.918	N_8	0.2076	N_8	0.1999
MPUT	0.52%	2.24%	1.821%	0.4921 %		2.152%		3.236%	
MPOT	0.8915%	2.94%	2.202%	0.963 %		2.921%		3.4572%	
T_{stl}	zero	zero	0.4003 s	zero		0.4284 s		0.4471 s	
E_{sse}	0.162%	0.203%	0.412%	0.3921 %		0.4412%		0.491%	
				Scenario 2 DG 3					
Optimal size	online	online	online	N_9	6.143	N_9	5.4976	N_9	0.8995
				N_{10}	0.0013	N_{10}	0.0068	N_{10}	0.0656
				N_{11}	2.4895	N_{11}	1.5785	N_{11}	1.4879
				N_{12}	0.895	N_{12}	0.1755	N_{12}	0.1625
MPUT	0.514%	2.11%	1.813%	0.498 %		2.072%		3.211%	
MPOT	0.891%	2.95%	2.197%	0.9471 %		2.906%		3.4362%	
T_{stl}	zero	zero	0.3941 s	zero		0.42331 s		0.418 s	
E_{sse}	0.162%	0.201%	0.403%	0.411 %		0.432%		0.486%	

TABLE 6. The outcomes of each DG for scenario 3 with AWGC-DA, EBS-ABA, LMSRE, COOT, PSO, and SFO techniques.

	AWGC-DA	EBS-ABA	LMSRE	COOT		SFO		PSO	
				Scenario 3 DG 1					
Optimal size	online	online	online	N_1	6.5	N_1	6.1344	N_1	2.1084
				N_2	0.001	N_2	0.0046	N_2	0.0062
				N_3	2.6	N_3	2.4985	N_3	2.575
				N_4	0.9	N_4	0.1216	N_4	0.113
MPUT	91.54%	92.05%	92.155%	92.11 %		91.651%		93.11%	
MPOT	7.55%	10.5%	12.36%	11.55 %		11.69%		11.971%	
T_{stl}	0.189 s	0.22 s	0.4912 s	0.2447sec		0.5661 s		0.812 s	
E_{sse}	0.195%	0.19%	0.257%	0.311 %		0.47%		0.549%	
				Scenario 3 DG 2					
Optimal size	online	online	online	N_5	6.365	N_5	6.231	N_5	2.179
				N_6	0.0012	N_6	0.0044	N_6	0.006
				N_7	2.586	N_7	2.5151	N_7	2.554
				N_8	0.9461	N_8	0.1193	N_8	0.099
MPUT	91.15%	91.17%	92.07%	91.612 %		91.598%		93.092%	
MPOT	7.41%	10.14%	12.31%	11.651 %		11.64%		11.89%	
T_{stl}	0.188 s	0.212 s	0.488 s	0.2446 s		0.5561 s		0.8061 s	
E_{sse}	0.193%	0.184%	0.2521%	0.3241 %		0.4687%		0.546%	
				Scenario 3 DG 3					
Optimal size	online	online	online	N_9	6.2121	N_9	6.1221	N_9	2.23
				N_{10}	0.00135	N_{10}	0.0046	N_{10}	0.0064
				N_{11}	2.523	N_{11}	2.4752	N_{11}	2.5131
				N_{12}	0.9671	N_{12}	0.1213	N_{12}	0.0109
MPUT	91.14%	91.17%	91.86%	91.261 %		91.432%		92.88%	
MPOT	7.398%	10.14%	12.22%	12.11 %		11.59%		11.83%	
T_{stl}	0.1876 s	0.212 s	0.483 s	0.2493 sec		0.552 s		0.795 s	
E_{sse}	0.191%	0.184%	0.25%	0.4341 %		0.4679%		0.5424%	

EBS-ABA, LMSRE, COOT, PSO, and SFO techniques. Notably, the MPUT for the autonomous status of the proposed method is less than 7.5% in Fig. 3a. Moreover, the proposed
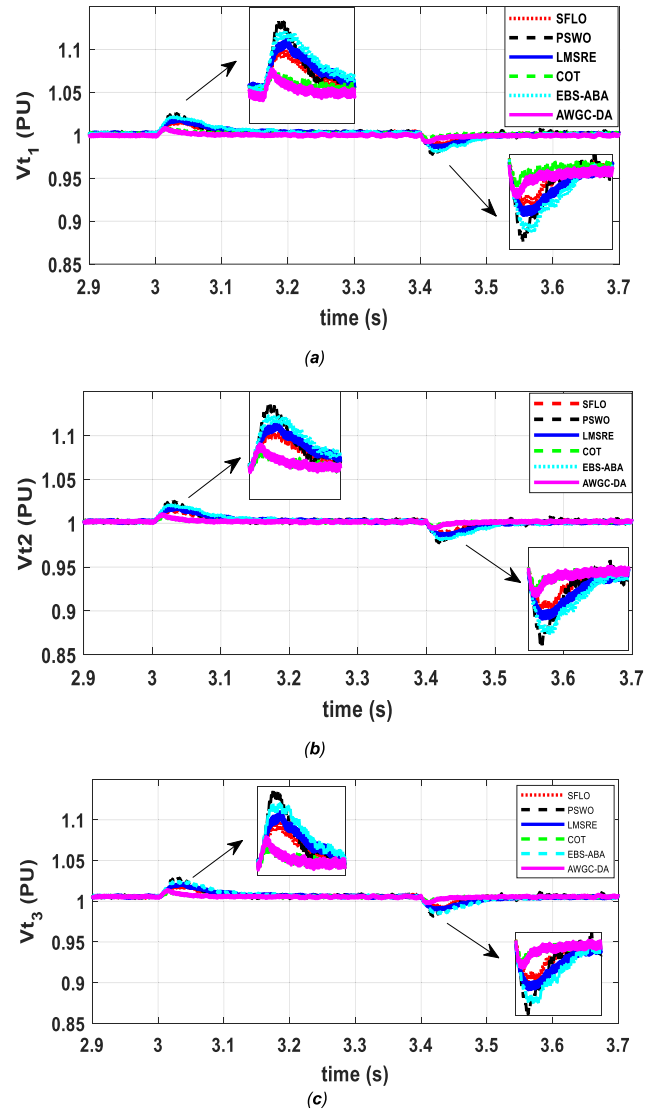

FIGURE 5. The profile voltages of, (a) DG1, (b) DG2, and (c) DG3 for scenario 2 with using AWGC-DA, EBS-ABA, LMSRE, COOT, PSO, and SFO techniques.

technique reduces the T_{stl} to 31 ms, satisfying the 2% criteria, and E_{sse} is 0.19%. Therefore, The suggested optimizer generates the fewest overshoots, the quickest damping, and the best E_{sse}. Importantly, in MPUT, T_{stl}, and E_{sse}, the AWGC-DA surpasses the EBS-ABA, LMSRE, COOT, PSO, and SFO approaches, indicating the solidity, reliability, and functionality of the proposed AWGC-DA over the EBS-ABA, LMSRE, COOT, PSO, and SFO methods.

B. SCENARIO 2 (VARIATIONS IN LOAD UNDER AUTONOMOUS STATUS)

The MG runs smoothly in the autonomous state in the second scenario. As illustrated in Table 1, the MG is initially developed with a complicated load. Then, at t = 3 s, R12 is increased to 300 and then decreased to 150 at t = 3.4 s. The optimum PI gains for the DGs using AWGC-DA, EBS-ABA,
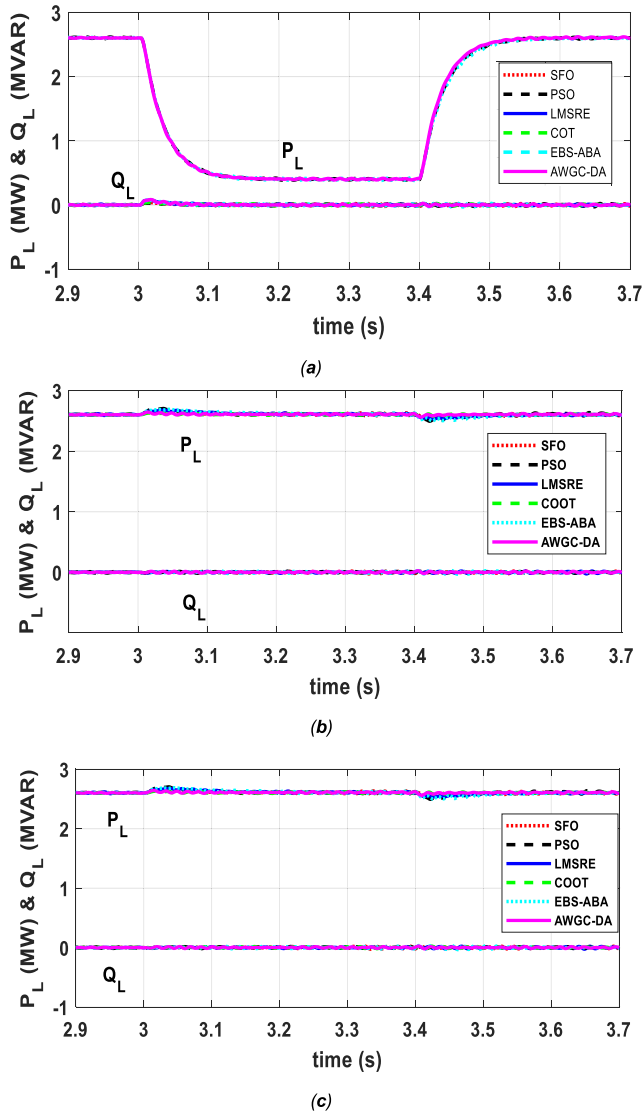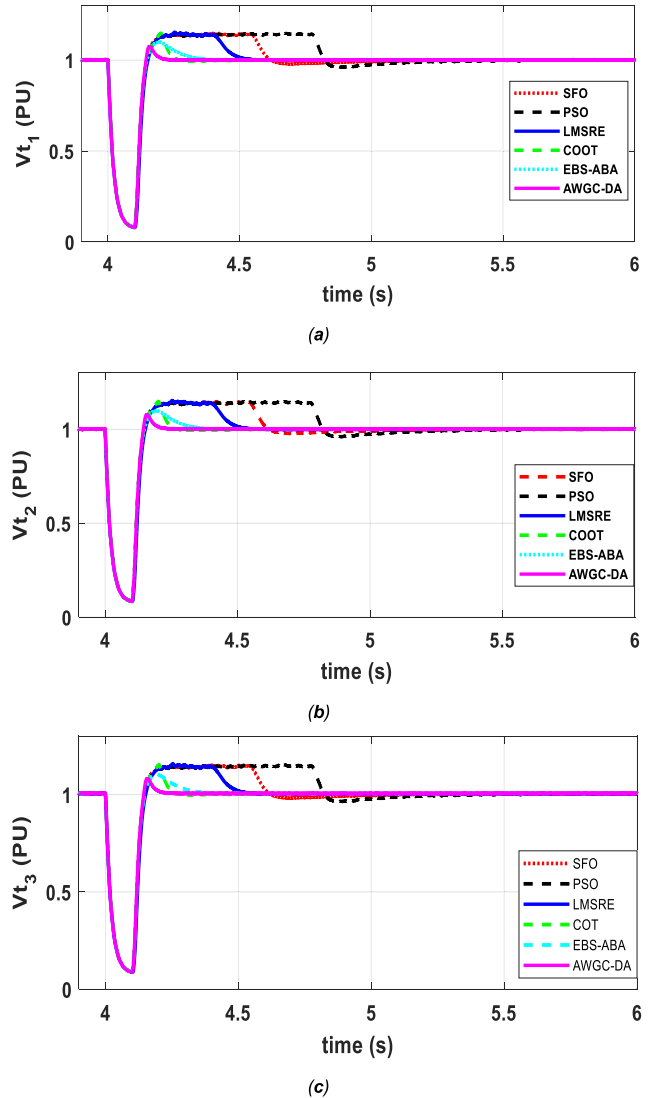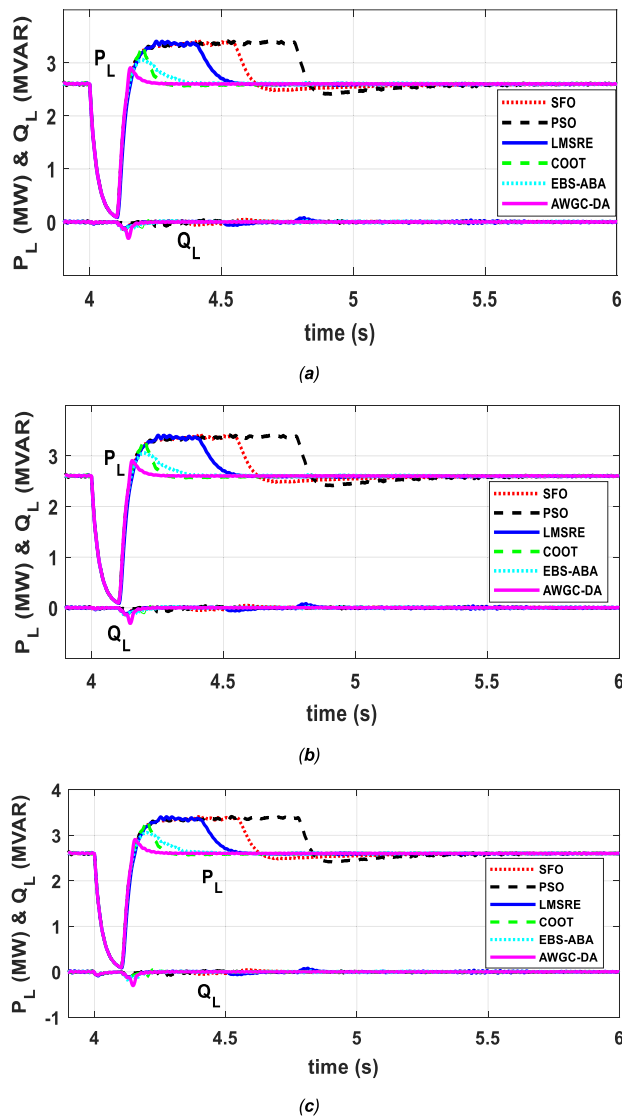
FIGURE 6. The load powers (P&Q) of, (a) DG1, (b) DG2, and (c) DG3 for scenario 2 with using AWGC-DA, EBS-ABA, LMSRE, COOT, PSO, and SFO techniques.

FIGURE 7. The profile voltages of, (a) DG1, (b) DG2, and (c) DG3 for scenario 3 with using AWGC-DA, EBS-ABA, LMSRE, COOT, PSO, and SFO techniques.

LMSRE, COOT, PSO, and SFO techniques are presented in Table 5. The voltage of the DGs using AWGC-DA and the other methods is compared in Figs. 5a-c. Additionally, Figs. 6a-c show the complex power in the DGs using AWGC-DA, EBS-ABA, LMSRE, COOT, PSO, and SFO techniques. Notably, the proposed controller reduces the T_{stl} to zero seconds in Figure 5a, satisfying the 2% criteria, and E_{sse} is 0.16%. Therefore, The suggested optimizer generates the fewest overshoots, the quickest damping, and the best E_{sse}. It is critical to notice that in Fig. 5a, the MPUT for the load variations scenario of the proposed technique is less than 0.55%. It is critical to recall that in Fig. 6a, DG1's active power is reduced to 1.3 MW and successfully restored at t = 3.4 s. Nonetheless, the rest of the DGs. Importantly, in MPOT, T_{stl}, and E_{sse}, the AWGC-DA surpasses the EBS-ABA, LMSRE, COOT, PSO, and SFO approaches, indicating the solidity, reliability, and functionality of the proposed

AWGC-DA over the EBS-ABA, LMSRE, COOT, PSO, and SFO methods.

C. SCENARIO 3 (A THREE-PHASE FAULT UNDER AUTONOMOUS STATUS)

Throughout scenario 3, the MG maintains a steady state throughout the autonomous mode. A three-phase fault develops at PCC 1 at t = 4 s and subsequently returns to its prior situation at t = 4.1 s. The optimal PI gains for the DGs using AWGC-DA, EBS-ABA, LMSRE, COOT, PSO, and SFO techniques are presented in Table 6. The voltage of the DGs using AWGC-DA and the other methods is compared in Figs. 7a-c. Additionally, Figs. 8a-c show the complex power in the DGs using AWGC-DA, EBS-ABA, LMSRE, COOT, PSO, and SFO techniques. Notably, the proposed controller reduces the T_{stl} to 18 ms in Fig. 7a, satisfying the 2% criteria, and E_{sse} is 0.195%. Therefore, The suggested optimizer generates the fewest overshoots, the quickest damping,

FIGURE 8. The load powers (P&Q) of, (a) DG1, (b) DG2, and (c) DG3 for scenario 3 with using AWGC-DA, EBS-ABA, LMSRE, COOT, PSO, and SFO techniques.

and the best E_{sse}. Importantly, in MPOT, T_{stl}, and E_{sse}, the AWGC-DA surpasses the EBS-ABA, LMSRE, COOT, PSO, and SFO approaches, indicating the solidity, reliability, and functionality of the proposed AWGC-DA over the EBS-ABA, LMSRE, COOT, PSO, and SFO methods.

VII. CONCLUSION

This paper offers a new technique for optimizing the gains of PI-Cs using AWGC-DA. The goal is to improve MG performance by taking into account Twelve PI-C parameters. The suggested approach's usefulness is proved by simulation results produced using the PSCAD/EMTDC program. The outcomes display that the proposed controller can successfully regulate the voltage profile while preserving active and reactive powers. Furthermore, the results show prompt dampening in transient responses, alongside a short settling time (T_{stl}) and a small steady-state error

(E_{sse}) under different MG operating scenarios, such as (1) disconnected from the utility grid (autonomous status); (2) variations in load while in autonomous status; and (3) a three-phase fault while in autonomous status. To validate the presented AWGC-DA technique, numerous simulations were conducted to assess its efficacy in the system's transient responses compared to other optimization strategies such as EBS-ABA, LMSRE-based adaptive control, COOT, SFO, and PSO approaches. The results showed significant improvements achieved by the AWGC-DA approach. Specifically. In scenario 1, the AWGC-DA approach reduced the voltage undershoot (MPUT) by 10%, 7%, 43%, and 64% compared to the EBS-ABA, LMSRE, SFO, and PSO approaches, respectively. In scenario 2, it reduced the settling time (T_{stl}) by 14%, 61.5%, 23%, 66.5%, and 76.7% relative to the EBS-ABA, LMSRE, COOT, SFO, and PSO approaches, respectively. In scenario 2, where the MG encountered a sudden load change under autonomous status, the presented approach achieved a T_{stl} of zero seconds, indicating a rapid response and stability. Moreover, In scenario 3, the AWGC-DA approach reduced the voltage overshoot (MPOT) by 28%, 39%, 35%, 35.4%, and 37% compared to the EBS-ABA, LMSRE, COOT, SFO, and PSO approaches, respectively. These results highlight the superior performance and efficacy of the AWGC-DA approach compared to other optimization strategies in improving system behavior during transient events

The suggested AWGC-DA will be improved in the future to be used in numerous fields such as electrical networks, battery storage approaches, and smart-grid, delivering the best outcomes in green energy systems. The experimental implementation of the proposed optimization techniques and the implementation on a real site will be considered in future work.

REFERENCES

[1] V. S. Tabar and V. Abbasi, "Energy management in microgrid with considering high penetration of renewable resources and surplus power generation problem," *Energy*, vol. 189, Dec. 2019, Art. no. 116264, doi: 10.1016/J.ENERGY.2019.116264.

[2] B. Alghamdi and C. Cañizares, "Frequency and voltage coordinated control of a grid of AC/DC microgrids," *Appl. Energy*, vol. 310, Mar. 2022, Art. no. 118427, doi: 10.1016/J.APENERGY.2021.118427.

[3] M. Uddin, M. F. Romlie, M. F. Abdullah, C. Tan, G. Shafiullah, and A. H. A. Bakar, "A novel peak shaving algorithm for islanded microgrid using battery energy storage system," *Energy*, vol. 196, Apr. 2020, Art. no. 117084, doi: 10.1016/J.ENERGY.2020.117084.

[4] C. D. Raj, D. N. Gaonkar, and J. M. Guerrero, "Improved *P-f/Q-V* and *P-V/Q-f* droop controllers for parallel distributed generation inverters in AC microgrid," *Sustain. Cities Soc.*, vol. 41, pp. 421–442, Aug. 2018, doi: 10.1016/J.SCS.2018.04.026.

[5] R. An, Z. Liu, J. Liu, and B. Liu, "A comprehensive solution to decentralized coordinative control of distributed generations in islanded microgrid based on dual-frequency-droop," *IEEE Trans. Power Electron.*, vol. 37, no. 3, pp. 3583–3598, Mar. 2022, doi: 10.1109/TPEL.2021.3115522.

[6] Z. Özkan and A. M. Hava, "Inductor saturation compensation in three-phase three-wire voltage-source converters via inverse system dynamics," *IEEE Trans. Ind. Electron.*, vol. 69, no. 5, pp. 4309–4319, May 2022, doi: 10.1109/TIE.2021.3084155.

[7] S. D'Arco, J. A. Suul, and O. B. Fosso, "Automatic tuning of cascaded controllers for power converters using eigenvalue parametric sensitivities," *IEEE Trans. Ind. Appl.*, vol. 51, no. 2, pp. 1743–1753, Mar. 2015, doi: 10.1109/TIA.2014.2354732.

[8] M. Saleh, Y. Esa, and A. Mohamed, "Centralized control for DC microgrid using finite state machine," in *Proc. IEEE Power Energy Soc. Innov. Smart Grid Technol. Conf. (ISGT)*, Apr. 2017, pp. 1–5, doi: 10.1109/ISGT.2017.8086062.

[9] W. S. W. Wang, D. E. Davison, and E. J. Davison, "Controller design for multivariable linear time-invariant unknown systems," *IEEE Trans. Autom. Control*, vol. 58, no. 9, pp. 2292–2306, Sep. 2013, doi: 10.1109/TAC.2013.2258812.

[10] Y. K. Bhateshvar and H. D. Mathur, "Power–frequency balance with superconducting magnetic energy storage using optimized intelligent controller," *Energetika*, vol. 60, no. 3, pp. 149–161, Nov. 2014, doi: 10.6001/ENERGETIKA.V60I3.2988.

[11] A. M. Hussien, R. A. Turky, A. Alkuhayli, H. M. Hasanien, M. Tostado-Véliz, F. Jurado, and R. C. Bansal, "Coot bird algorithms-based tuning PI controller for optimal microgrid autonomous operation," *IEEE Access*, vol. 10, pp. 6442–6458, 2022, doi: 10.1109/ACCESS.2022.3142742.

[12] A. M. Taher, H. M. Hasanien, A. R. Ginidi, and A. T. M. Taha, "Hierarchical model predictive control for performance enhancement of autonomous microgrids," *Ain Shams Eng. J.*, vol. 12, no. 2, pp. 1867–1881, Jun. 2021, doi: 10.1016/J.ASEJ.2020.12.007.

[13] S. Patel, B. Mohanty, and H. M. Hasanien, "Competition over resources optimized fuzzy TIDF controller for frequency stabilization of hybrid micro-grid system," *Int. Trans. Electr. Energy Syst.*, vol. 30, no. 9, p. e12513, Sep. 2020, doi: 10.1002/2050-7038.12513.

[14] I. Boussaïd, J. Lepagnot, and P. Siarry, "A survey on optimization metaheuristics," *Inf. Sci.*, vol. 237, pp. 82–117, Jul. 2013, doi: 10.1016/J.INS.2013.02.041.

[15] M. A. M. Shaheen, Z. Ullah, H. M. Hasanien, M. Tostado-Véliz, H. Ji, M. H. Qais, S. Alghuwainem, and F. Jurado, "Enhanced transient search optimization algorithm-based optimal reactive power dispatch including electric vehicles," *Energy*, vol. 277, Aug. 2023, Art. no. 127711, doi: 10.1016/J.ENERGY.2023.127711.

[16] M. A. M. Shaheen, Z. Ullah, M. H. Qais, H. M. Hasanien, K. J. Chua, M. Tostado-Véliz, R. A. Turky, F. Jurado, and M. R. Elkadeem, "Solution of probabilistic optimal power flow incorporating renewable energy uncertainty using a novel circle search algorithm," *Energies*, vol. 15, no. 21, p. 8303, Nov. 2022, doi: 10.3390/EN15218303.

[17] M. A. M. Shaheen, H. M. Hasanien, S. F. Mekhamer, M. H. Qais, S. Alghuwainem, Z. Ullah, M. Tostado-Véliz, R. A. Turky, F. Jurado, and M. R. Elkadeem, "Probabilistic optimal power flow solution using a novel hybrid metaheuristic and machine learning algorithm," *Mathematics*, vol. 10, no. 17, p. 3036, Aug. 2022, doi: 10.3390/MATH10173036.

[18] I. Alsaidan, M. A. M. Shaheen, H. M. Hasanien, M. Alaraj, and A. S. Alnafisah, "A PEMFC model optimization using the enhanced bald eagle algorithm," *Ain Shams Eng. J.*, vol. 13, no. 6, Nov. 2022, Art. no. 101749, doi: 10.1016/J.ASEJ.2022.101749.

[19] I. A. Ayad, E. Elwarraki, S. U. Ali, S. M. Qaisar, A. Waqar, M. Baghdadi, and A. Alzahrani, "Optimized nonlinear integral backstepping controller for DC–DC three-level boost converters," *IEEE Access*, vol. 11, pp. 49794–49805, 2023, doi: 10.1109/ACCESS.2023.3274773.

[20] J. Hu, W. Cao, F. Jiang, L. Hu, Q. Chen, W. Zheng, and J. Zhou, "Study on multi-objective optimization of power system parameters of battery electric vehicles," *Sustainability*, vol. 15, no. 10, p. 8219, May 2023, doi: 10.3390/SU15108219.

[21] A. Ali, M. F. Shaaban, A. Abdelfatah, M. A. Azzouz, and A. S. A. Awad, "Optimal allocation of FCSs and PV units in smart grids considering traffic and generation dispatch," *Sustain. Energy, Grids Netw.*, vol. 34, Jun. 2023, Art. no. 101063, doi: 10.1016/J.SEGAN.2023.101063.

[22] H. Ren, X. Hou, Z. Jia, and A. Mashhadi, "A new optimal energy management strategy of microgrids using chaotic map-based chameleon swarm algorithm," *IET Renew. Power Gener.*, vol. 17, no. 8, pp. 1978–1992, May 2023, doi: 10.1049/RPG2.12744.

[23] A. M. Hussien, H. M. Hasanien, and S. F. Mekhamer, "Sunflower optimization algorithm-based optimal PI control for enhancing the performance of an autonomous operation of a microgrid," *Ain Shams Eng. J.*, vol. 12, no. 2, pp. 1883–1893, Jun. 2021, doi: 10.1016/J.ASEJ.2020.10.020.

[24] N. M. Neamah, A. Abuhussein, A. Hossam-Eldin, S. Alghamdi, and K. M. AboRas, "Improvement of frequency regulation of a wind-integrated power system based on a PD-PIDA controlled STATCOM tuned by the artificial rabbits optimizer," *IEEE Access*, vol. 11, pp. 55716–55735, 2023, doi: 10.1109/ACCESS.2023.3277202.

[25] A. M. Hussien, S. F. Mekhamer, and H. M. Hasanien, "Cuttlefish optimization algorithm based optimal PI controller for performance enhancement of an autonomous operation of a DG system," in *Proc. 2nd Int. Conf. Smart Power Internet Energy Syst. (SPIES)*, Sep. 2020, pp. 293–298, doi: 10.1109/SPIES48661.2020.9243093.

[26] M. Y. Abdel-Kader, A. M. Ebid, K. C. Onyelowe, I. M. Mahdi, and I. Abdel-Rasheed, "(AI) in infrastructure projects—Gap study," *Infrastructures*, vol. 7, no. 10, p. 137, Oct. 2022, doi: 10.3390/INFRASTRUCTURES7100137.

[27] Y. Xi, X. Tang, Z. Li, Y. Cui, T. Zhao, X. Zeng, J. Guo, and W. Duan, "Harmonic estimation in power systems using an optimised adaptive Kalman filter based on PSO-GA," *IET Gener., Transmiss. Distrib.*, vol. 13, no. 17, pp. 3968–3979, Sep. 2019, doi: 10.1049/IET-GTD.2018.6148.

[28] R. Saleh, "A comparative study of particle swarm optimized control techniques for active suspension system," *Int. Rev. Autom. Control*, vol. 15, no. 4, pp. 213–221, Jul. 2022, doi: 10.15866/IREACO.V15I4.22430.

[29] M. A. R. Shafei, D. K. Ibrahim, and M. Bahaa, "Application of PSO tuned fuzzy logic controller for LFC of two-area power system with redox flow battery and PV solar park," *Ain Shams Eng. J.*, vol. 13, no. 5, Sep. 2022, Art. no. 101710, doi: 10.1016/J.ASEJ.2022.101710.

[30] V. Veerasamy, N. I. A. Wahab, R. Ramachandran, M. L. Othman, H. Hizam, A. X. R. Irudayaraj, J. M. Guerrero, and J. S. Kumar, "A Hankel matrix based reduced order model for stability analysis of hybrid power system using PSO-GSA optimized cascade PI-PD controller for automatic load frequency control," *IEEE Access*, vol. 8, pp. 71422–71446, 2020, doi: 10.1109/ACCESS.2020.2987387.

[31] G. Yuan and W. Yang, "Study on optimization of economic dispatching of electric power system based on hybrid intelligent algorithms (PSO and AFSA)," *Energy*, vol. 183, pp. 926–935, Sep. 2019, doi: 10.1016/J.ENERGY.2019.07.008.

[32] J. Chang, Z. Li, Y. Huang, X. Yu, R. Jiang, R. Huang, and X. Yu, "Multi-objective optimization of a novel combined cooling, dehumidification and power system using improved M-PSO algorithm," *Energy*, vol. 239, Jan. 2022, Art. no. 122487, doi: 10.1016/J.ENERGY.2021.122487.

[33] S. Surender Reddy and P. R. Bijwe, "Efficiency improvements in meta-heuristic algorithms to solve the optimal power flow problem," *Int. J. Electr. Power Energy Syst.*, vol. 82, pp. 288–302, Nov. 2016, doi: 10.1016/J.IJEPES.2016.03.028.

[34] X. Wang and J. Han, "Affine projection algorithm based on least mean fourth algorithm for system identification," *IEEE Access*, vol. 8, pp. 11930–11938, 2020, doi: 10.1109/ACCESS.2020.2966038.

[35] J. Sung Lim, "New adaptive filtering algorithms based on an orthogonal projection of gradient vectors," *IEEE Signal Process. Lett.*, vol. 7, no. 11, pp. 314–316, Nov. 2000, doi: 10.1109/97.873568.

[36] S. Werner and P. S. R. Diniz, "Set-membership affine projection algorithm," *IEEE Signal Process. Lett.*, vol. 8, no. 8, pp. 231–235, Aug. 2001, doi: 10.1109/97.935739.

[37] H. E. Keshta, A. A. Ali, O. P. Malik, E. M. Saied, and F. M. Bendary, "Adaptive control strategy for improved dynamic performance of two islanded inter-connected micro-grids," *Int. J. Electr. Power Energy Syst.*, vol. 126, Mar. 2021, Art. no. 106562, doi: 10.1016/J.IJEPES.2020.106562.

[38] A. M. Hussien, R. A. Turky, H. M. Hasanien, and A. Al-Durra, "LMSRE-based adaptive PI controller for enhancing the performance of an autonomous operation of microgrids," *IEEE Access*, vol. 9, pp. 90577–90586, 2021, doi: 10.1109/ACCESS.2021.3091496.

[39] H. M. Hasanien, "An adaptive control strategy for low voltage ride through capability enhancement of grid-connected photovoltaic power plants," *IEEE Trans. Power Syst.*, vol. 31, no. 4, pp. 3230–3237, Jul. 2016, doi: 10.1109/TPWRS.2015.2466618.

[40] M. A. Soliman, H. M. Hasanien, A. Al-Durra, and I. Alsaidan, "A novel adaptive control method for performance enhancement of grid-connected variable-speed wind generators," *IEEE Access*, vol. 8, pp. 82617–82629, 2020, doi: 10.1109/ACCESS.2020.2991689.

[41] H. K. Shaker, H. E. Keshta, M. A. Mosa, and A. A. Ali, "Adaptive nonlinear controllers based approach to improve the frequency control of multi islanded interconnected microgrids," *Energy Rep.*, vol. 9, pp. 5230–5245, Dec. 2023, doi: 10.1016/J.EGYR.2023.04.007.

[42] H. M. Hasanien, R. A. Turky, M. Tostado-Véliz, S. M. Muyeen, and F. Jurado, "Enhanced block-sparse adaptive Bayesian algorithm based control strategy of superconducting magnetic energy storage units for wind farms power ripple minimization," *J. Energy Storage*, vol. 50, Jun. 2022, Art. no. 104208, doi: 10.1016/J.EST.2022.104208.

[43] H. Zayyani and M. Korki, "Adaptive-width generalized correntropy diffusion algorithm for secure distributed estimation," *IEEE Trans. Circuits Syst. II, Exp. Briefs*, vol. 70, no. 7, pp. 2700–2704, Jul. 2023, doi: 10.1109/TCSII.2023.3242092.

[44] H. M. Hasanien, A. S. Abd-Rabou, and S. M. Sakr, "Design optimization of transverse flux linear motor for weight reduction and performance improvement using response surface methodology and genetic algorithms," *IEEE Trans. Energy Convers.*, vol. 25, no. 3, pp. 598–605, Sep. 2010, doi: 10.1109/TEC.2010.2050591.

[45] I. Y. Kim and O. L. de Weck, "Adaptive weighted sum method for multiobjective optimization: A new method for Pareto front generation," *Struct. Multidisciplinary Optim.*, vol. 31, no. 2, pp. 105–116, Feb. 2006, doi: 10.1007/S00158-005-0557-6/METRICS.

[46] A. H. Sayed, "Adaptation, learning, and optimization over networks," *Found. Trends Mach. Learn.*, vol. 7, nos. 4–5, pp. 311–801, 2014, doi: 10.1561/2200000051.

[47] A. M. Hussien, J. Kim, A. Alkuhayli, M. Alharbi, H. M. Hasanien, M. Tostado-Véliz, R. A. Turky, and F. Jurado, "Adaptive PI control strategy for optimal microgrid autonomous operation," *Sustainability*, vol. 14, no. 22, p. 14928, Nov. 2022, doi: 10.3390/SU142214928.

AHMED M. HUSSIEN received the B.Sc. degree in electrical engineering from the Faculty of Engineering, Future University in Egypt, Cairo, Egypt, in 2014, and the M.Sc. degree in electrical engineering from the Faculty of Engineering, Ain Shams University, Cairo, in 2021, where he is currently pursuing the Ph.D. degree. He is currently an Assistant Lecturer with the Faculty of Engineering, Future University in Egypt. His research interests include power systems operation, energy storage systems, energy management, and renewable energy systems.

HANY M. HASANIEN (Senior Member, IEEE) received the B.Sc., M.Sc., and Ph.D. degrees in electrical engineering from the Faculty of Engineering, Ain Shams University, Cairo, Egypt, in 1999, 2004, and 2007, respectively. From 2008 to 2011, he was a Joint Researcher with the Kitami Institute of Technology, Kitami, Japan. From 2012 to 2015, he was an Associate Professor with the College of Engineering, King Saud University, Riyadh, Saudi Arabia. Currently, he is a Professor with the Electrical Power and Machines Department, Faculty of Engineering, Ain Shams University. His research interests include modern control techniques, power systems dynamics and control, energy storage systems, renewable energy systems, and smart grid. He is an Editorial Board Member of *Electric Power Components and Systems Journal*. He is a Subject Editor of *IET Renewable Power Generation* and *Frontiers in Energy Research and Electronics* (MDPI). He has authored, coauthored, and edited three books in the field of electric machines and renewable energy. He has published more than 250 papers in international journals and conferences. His biography has been included in *Marquis Who's Who in the World* for its 28 edition, in 2011. He was awarded the Encouraging Egypt Award for Engineering Sciences, in 2012. He was awarded Institutions Egypt Award for Invention and Innovation of Renewable Energy Systems Development, in 2014. He was awarded the Superiority Egypt Award for Engineering Sciences, in 2019. He was received the Ain Shams University Appreciation Award in Engineering Sciences for 2022. He was the IEEE PES Egypt Chapter Chair (2020–2022). He is also the Editor-in-Chief of *Ain Shams Engineering Journal* (Elsevier).

MOHAMMED H. QAIS (Member, IEEE) received the B.Sc. degree in electrical engineering from Sana'a University, Yemen, in 2007, and the M.Sc. and Ph.D. degrees in electrical engineering from King Saud University, Saudi Arabia, in 2014 and 2020, respectively. Since August 2021, he has been a Postdoctoral Fellow with the Centre for Advances in Reliability and Safety Ltd. (CAiRS), Hong Kong, China. From June 2020 to June 2021, he was a Postdoctoral Researcher with the Electrical Engineering Department, King Saud University. From 2008 to 2011, he was an Electrical Engineer with Yemen Mobile Company, Yemen. Since 2011, he has been a Lecturer (on leave) with the Electrical Engineering Department, Sana'a University. His research interests include the AI-based control of grid-connected renewable energy power plants, microgrids, energy management, power system operation and control, and power system protection.

SAAD ALGHUWAINEM (Senior Member, IEEE) received the B.Sc. degree in electrical engineering from King Saud University, Riyadh, Saudi Arabia, in 1974, the M.Sc. degree in electrical engineering from the University of Colorado, Boulder, in 1978, and the Ph.D. degree in electrical engineering from the University of Michigan, Ann Arbor, 1986. Since 1986, he has been with the Department of Electrical Engineering, King Saud University, where he is currently a Professor. His research interests include renewable energy, power systems operation, control and optimization, power system protection, and electromagnetic transients.

● ● ●